An Investigation of the Laser Refrigeration Assisted Surface-Enhanced Raman Sepectrocopy by Gold Nanorods with Specified Plamonic Wavelength

Zhaojie Feng

A thesis

submitted in partial fulfillment of the

requirements for the degree of

Master of Science

University of Washington

2023

Committee:

Peter J. Pauzauskie

Bruce J. Hinds

Program Authorized to Offer Degree:

Materials Science and Engineering

University of Washington

Abstract

An Investigation of the Laser Refrigeration Assisted Surface-Enhanced Raman Sepectrocopy by Gold Nanorods with Specified Plamonic Wavelength

Zhaojie Feng

Chair of the Supervisory Committee:
Peter J. Pauzauskie
Department of Materials Science and Engineering

Surface-Enhanced Raman spectroscopy (SERS) technique largely broaden the application of Raman spectroscopy, which is a powerful analytical technique that provides valuable insights into the molecular composition and structure of a wide range of materials. Here, we synthesize a gold nanorods with specific plasmonic resonance at both 532nm and 1020nm to obtain excellent Raman enhance ability which can be further improved by combining the ytterbium doped Sodium Yttrium Fluoride ($NaYF:Yb^{3+}$) to possess laser refrigeration capability that may allow high laser power as well as better resolution under same experimental conditions.

This article used scanning electron microscopy and transmission electron microscopy to characterize the synthesized gold nanorods (AuNRs). After confirming the aspect ratio is about 6.6 ± 1.6, the UV-Vis spectrometer is used to collect the plasmonic resonance peak of the AuNRs which is at 519nm and 1017nm respectively. Furthermore, two target molecules includes rhodamine 6G (R6G) and Bovine Serum Albumin (BSA) were used for the SERS ability investigation. Moreover, this article innovatively applied anti-stokes/stokes Raman ratio as a nano thermometer to acquire the in-situ temperature information of the system, which preliminary confirm the possibility of cooling the system and protecting the sample while the Raman spectrum collection.

TABLE OF CONTENTS

LIST OF FIGURES

ACKNOWLEDGEMENTS

I would like to express my deepest gratitude and appreciation to Professor Peter Pauzauskie for his invaluable guidance, unwavering support, and exceptional mentorship throughout the completion of this master's thesis. I would also like to extend my gratitude to the members, Professor Bruce J. Hinds of my thesis committee for their valuable input and feedback. Their expertise and insights have been instrumental in shaping the final outcome of this research endeavor.

I would like to extend my sincere gratitude to the esteemed Dr. Greg Felsted and Chaman Gupta for their invaluable guidance and support in navigating the complexities of the optics table. I am also deeply grateful to Alex Bard and Rachel Gariepy for their unwavering professionalism and robust assistance with TEM microscopy. Additionally, I would like to express my heartfelt appreciation to Lars Forberger and Sankhya Hirani for their exceptional work in the field of SEM microscopy. Last but certainly not least, my profound thanks go to Chris Woodburn and Alexey Soldatenko for their invaluable guidance and expertise in the realm of Raman spectroscopy.

A special thanks to my family, their unfailing support are with me in whatever I pursue.

Chapter 1 – INTRODUCTION

1.1. Backgound of Surface enhanced Raman Spectroscopy

Surface-Enhanced Raman Spectroscopy (SERS) is a highly sensitive analytical technique that combines the inherent sensitivity of Raman spectroscopy with the enhanced signal obtained from nanostructured metallic surfaces. It has gained significant attention in recent years due to its ability to detect and characterize trace amounts of molecules, making it a valuable tool in various scientific and technological applications.

Raman spectroscopy is a non-destructive optical technique that provides molecular fingerprint information based on the inelastic scattering of light. It relies on the interaction between incident photons and molecular vibrations, resulting in a unique Raman spectrum that represents the molecular composition and structural information of the sample. However, conventional Raman spectroscopy often suffers from limited sensitivity, especially when dealing with low-concentration analytes or weakly scattering samples.

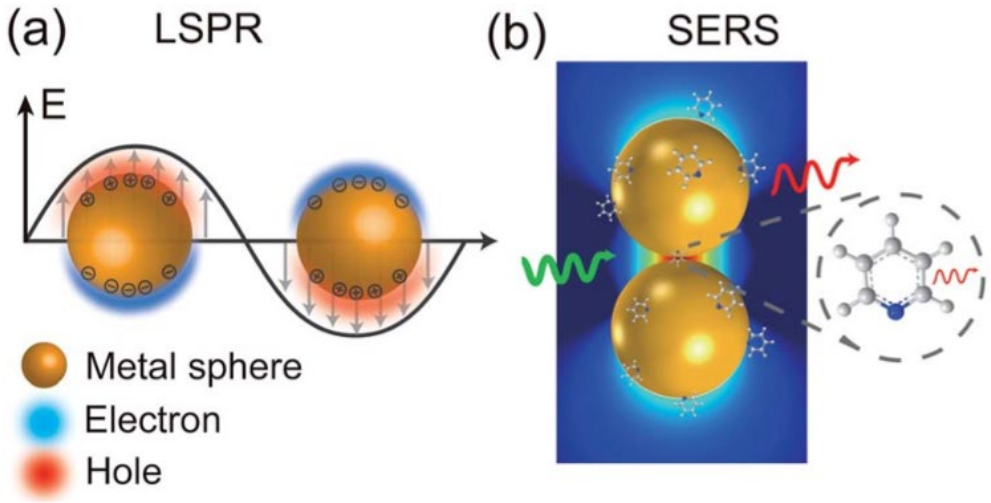

Figure 1. (a) Schematic diagrams of Localized Surface Plasmon Resonance (LSPR) (b) Diagrams of nanoparticle-molecule interactions[1].

The concept of surface enhancement in Raman spectroscopy was first proposed in the 1970s[2–5] when it was observed that the Raman signal from molecules in close proximity to certain roughened metal surfaces could be significantly enhanced. The enhancement arises from two main mechanisms: electromagnetic enhancement and chemical enhancement.

Electromagnetic enhancement is achieved through the excitation of localized surface plasmons in metallic nanostructures, such as nanoparticles, nanowires, or nanostructured films. When these metallic structures are illuminated by light, the collective oscillation of conduction electrons, known as surface plasmons, can significantly amplify the local electric field at the metal surface[5,6]. This enhanced field interacts with the nearby molecules, leading to a substantial increase in the Raman scattering cross-section, resulting in stronger Raman signals.

To achieve surface enhancement, various strategies have been employed to fabricate SERS-active substrates. These strategies include top-down approaches, such as electron beam lithography and focused ion beam milling, and bottom-up approaches, such as self-assembly techniques and colloidal nanoparticle synthesis. These techniques enable the precise control of the nanostructures size, shape, and composition to optimize the SERS enhancement. SERS has found widespread applications in diverse fields, including biomedical diagnostics, environmental monitoring, food safety, and forensic analysis. In biomedicine, SERS can be used for label-free detection and characterization of biomolecules, such as DNA, proteins, and drugs, enabling sensitive and specific diagnostics[7]. Environmental monitoring benefits from SERS by detecting and quantifying pollutants, heavy metals, and pesticides in complex samples. Additionally, SERS has been used in food safety to identify contaminants and ensure the quality of food products. In forensic analysis, SERS offers rapid and sensitive detection of trace evidence, including drugs, explosives, and counterfeit materials[8–11].

Despite the tremendous potential of SERS, several challenges remain, including reproducibility of the SERS signals, standardization of measurements, and the development of robust and cost-effective

substrates. Efforts are being made to overcome these challenges through advancements in nanofabrication techniques, substrate design, and improved instrumentation.

In conclusion, surface-enhanced Raman spectroscopy has revolutionized the field of molecular analysis by providing significantly enhanced sensitivity, allowing for the detection and characterization of analytes at trace levels. Its unique combination of sensitivity, selectivity, and versatility has made it a promising tool in a wide range of applications. Continued research and development in SERS are expected to further enhance its capabilities and enable its integration into various analytical platforms.

1.2. The phenomenon of Laser cooling

The quest for exploring the frontiers of science has driven researchers to delve into the realm of ultra-cold temperatures. In recent decades, laser cooling has emerged as a groundbreaking technique that has revolutionized the field of atomic physics. Among the various laser cooling methods, the application of lanthanide elements has garnered significant attention due to their unique properties and potential for achieving extremely low temperatures[12,13]. Lanthanide laser cooling is a cutting-edge technology that exploits the interaction between light and matter to achieve ultra-cold temperatures, unlocking a myriad of possibilities for fundamental research and technological advancements.

Lanthanides exhibit unique optical transitions that allow for efficient laser cooling. These transitions often involve narrow spectral lines in the near-infrared or visible range, making them suitable for laser manipulation. Two commonly employed laser cooling schemes for lanthanides are resolved sideband cooling and Raman cooling. Resolved sideband cooling relies on the ability to drive transitions between different atomic states using laser beams, while Raman cooling exploits the coupling between two internal atomic levels induced by lasers of different frequencies.

The advancements in lanthanide laser cooling hold immense potential for various scientific and technological applications. Ultra-cold lanthanide atoms can be used to study fundamental physics phenomena, including quantum magnetism, strongly correlated systems, and quantum simulation.

Furthermore, they are also being investigated for their potential in creating precise atomic clocks, quantum information processing, and quantum sensing applications[14–17].

1.3. Introduction of Nano thermometry

The ability to accurately measure temperature at the nanoscale is of paramount importance in various fields, including nanotechnology, materials science, and biomedicine. Conventional thermometry techniques often face limitations in terms of spatial resolution and sensitivity when applied to nanoscale systems. However, recent advancements in laser cooling techniques have opened up new possibilities for nano thermometry, enabling the precise measurement of temperature at the nanoscale[18]. This essay explores the emerging field of nano thermometry within the context of laser cooling, discussing the underlying principles, experimental techniques, and the immense potential of this approach in unraveling temperature-dependent phenomena in nanoscale systems.

Conventional thermometry techniques rely on macroscopic measurements, making it challenging to accurately assess temperature at the nanoscale. Nanoscale systems exhibit unique characteristics, such as localized heating and strong temperature gradients, requiring high-resolution thermometry methods. Moreover, the presence of thermal interfaces and fluctuations in thermal conductivity pose additional challenges in obtaining precise temperature measurements.

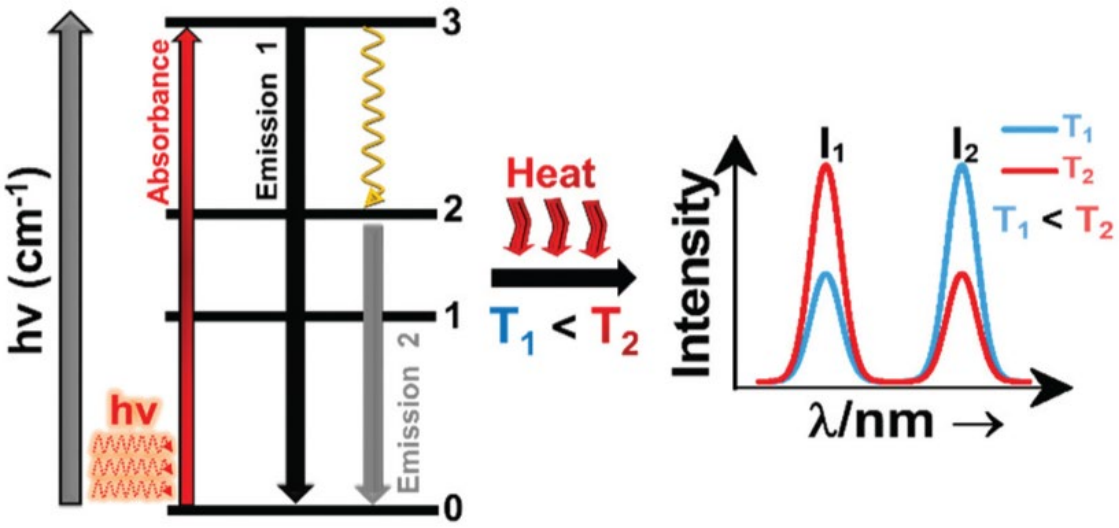

Figure 2. Basic working principle of luminescence nanothermometry[19].

Laser cooling offers several advantages for nanoscale thermometry. By employing carefully tuned laser beams, the motion of nanoscale objects, such as nanoparticles, can be effectively controlled. The absorption and re-emission of photons can be harnessed to extract valuable information about the temperature of the system[20]. Additionally, laser cooling allows for localized cooling, making it possible to measure temperatures at specific points within nanoscale structures.

Various experimental techniques have been developed to implement laser cooling for nano thermometry. These techniques often involve integrating temperature-sensitive nanoscale probes, such as nanoparticles or quantum dots, into the system of interest. The absorption and emission characteristics of these probes are influenced by temperature variations, providing a means to indirectly measure temperature. Moreover, advanced spectroscopic methods, including fluorescence lifetime imaging[21,22] and Raman scattering, can be employed to enhance the precision and sensitivity of temperature measurements.

Nano thermometry powered by laser cooling represents a promising frontier in the measurement of temperature at the nanoscale. By leveraging the principles of laser cooling, researchers can achieve unprecedented control over temperature-sensitive nanoscale systems. The integration of advanced

spectroscopic techniques and temperature-sensitive nanoscale probes opens up exciting opportunities for studying temperature-dependent phenomena in nanotechnology, materials science, and biomedicine. As research in this field progresses, nano thermometry through laser cooling is expected to pave the way for transformative advancements and insights into the fascinating world of nanoscale temperature dynamics.

1.4. Objective

Raman spectroscopy has emerged as a powerful technique that provides unique insights into molecular composition, bonding, and vibrational behavior. By harnessing the principles of light-matter interactions, Raman spectroscopy enables the identification and analysis of molecular fingerprints, offering a wealth of information about the chemical and physical properties of a wide range of materials.

Surface-enhanced Raman spectroscopy (SERS) is also a powerful technique that enhances the sensitivity and signal strength of traditional Raman spectroscopy by many orders of magnitude. It involves the interaction of molecules with specially designed metallic surfaces or nanostructures, resulting in an amplified Raman signal. SERS offers several advantages over conventional Raman spectroscopy, making it a valuable tool in various scientific and technological applications.

First, SERS provides a significant enhancement in sensitivity, allowing for the detection and analysis of molecules at extremely low concentrations. The electromagnetic field enhancement, known as the "surface-enhanced effect," occurs when molecules are in close proximity to metallic surfaces or nanostructures. This enhanced sensitivity enables the detection of trace amounts of analytes, making SERS particularly useful in applications requiring high sensitivity, such as trace chemical detection and biomedical diagnostics. Second, SERS can be applied to a wide range of sample types, including solids, liquids, and gases. It offers versatility in terms of experimental setups and measurement conditions, allowing for analysis in various environments, such as ambient conditions or under extreme temperatures and pressures. Moreover, SERS can be coupled with other analytical techniques, such as

microscopy, chromatography, and electrochemistry, further expanding its capabilities and enabling multimodal analysis. Furthermore, the SERS technique offers high spatial resolution, enabling the analysis of molecules at the nanoscale. It allows for the probing of molecular behavior and interactions in complex systems, such as at the interfaces of materials or within biological cells. Additionally, the SERS enhancement is highly dependent on the characteristics of the metallic substrate or nanostructures used, offering tunability in terms of enhancement factors and selectivity, enabling tailored and optimized analyses. As described, SERS overcomes the limitations of conventional Raman spectroscopy by providing significant sensitivity enhancement, molecular specificity, versatility, and non-destructive analysis. These advantages make SERS an indispensable technique for a wide range of applications, where high sensitivity, molecular identification, and nanoscale characterization are essential.

For SERS spectrum collection, the laser power and exposure time is the two main parameters which effect the result. Lowering the acquisition time to hundreds of milliseconds would allow the system to become more portable and efficient. Further, when the Raman spectrum was used as a tool in high-throughput scenario, it is imperative to have a quicker exposure time. However, the competing relationship between these two parameters restrain the possibility to allow the infinity reduction of the time. In other words, the laser power needed to rise, which will potentially make a major damage to the sample, especially when we are detecting biospecimen and ultra-low concentrations samples. Therefore, in order to protect the sample and further enhanced the resolution of the SERS system, it is innovative to combine the laser cooling materials with the gold nanorods which could achieve local cooling and in-situ nano thermometry.

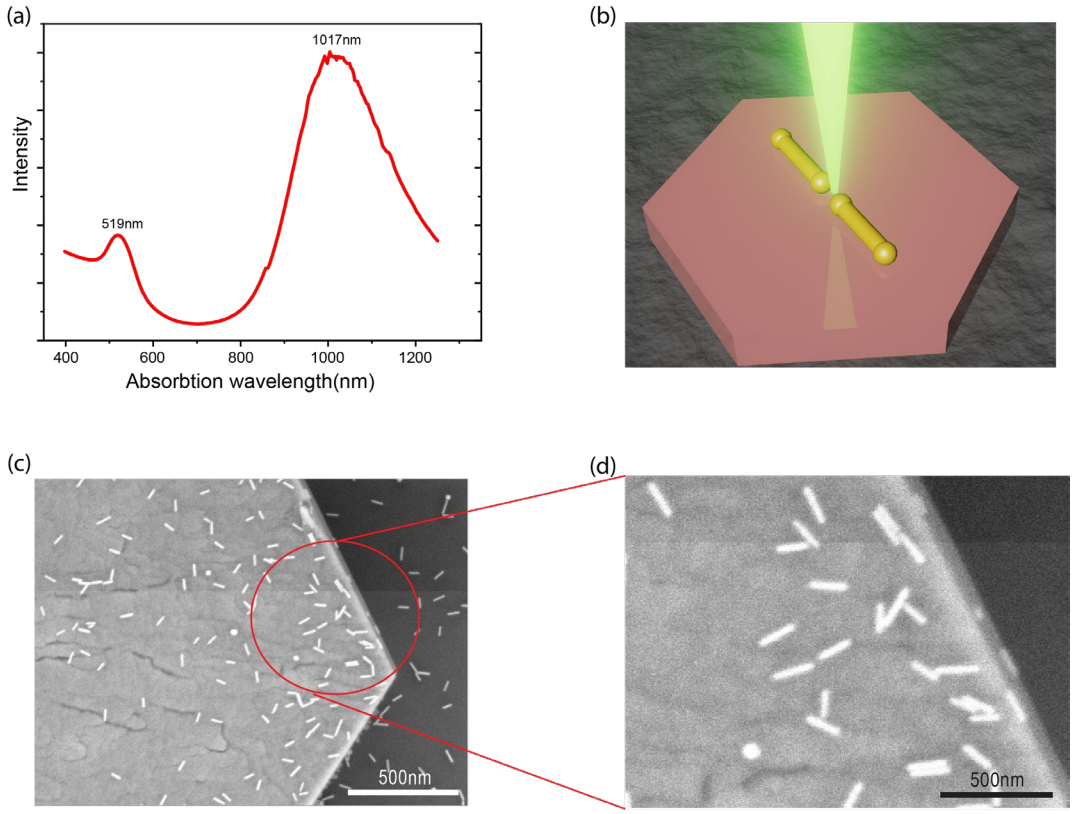

Figure 3. (a) UV-Vis spectrum showing the absorption peaks respectively correspond to the transverse and longitudinal plasmon resonance of synthesis AuNR. (b) Schematic showing the AuNR on the NaYF nanoparticle, creating a "hot-spot" which enables the Raman spectrum enhancement, while the laser introduces heat that could melt the gold nanorods and present a dumbbell shape. (c) SEM image of the AuNR deposit on the NaYF nanoparticle. (d) enlarged SEM image showing the "hot spot" which corresponds to the panel b).

To achieve the goal of collecting Raman spectrum under high power while cooling the sample and substrate, a unique gold nanorods are needed as a Raman enhancement and cooling enhancement agent. As shown in the **Figure 1. (a)**, the gold nanorods were designed to obtain two plasmonic resonance wavelengths at around 532nm and 1020nm respectively. Since the plasmon resonance has transvers mode and longitudinal mode, which are dependent on the width and length respectively, the second absorption wavelength are deliberately manipulated at the wavelength of 1020nm to corporate with the laser cooling excitation. The NaYF: Yb^{3+} nanoparticles act as the cooling substrate, in fact, the ytterbium doped NaYF nanoparticles have been used as a laser cooling material for a long time. Researchers are designing various way to control the morphology and doping density of the particles to try to improve the cooling performance. **Figure 1. (b)** shows the schematic of the ideal experimental setup, which indicates the micron scale size and prism shape has made the NaYF particle suitable for acting as the

substrate for gold nanorods. When the incident laser hit the gold nanorods, it will generate huge amounts of heat that will potentially melt the gold nanorods into a dumbbell shape. This effect will change the plasmonic wavelength and largely reduce the Raman enhance performance. **Figure 1. (c) and (d)** is the SEM image showing the exact morphology perfectly matches the schematic, which paves the way for the accomplishment of combining laser cooling and SERS to protect the sample while collecting as much signal as possible.

Furthermore, the other advantage of this system is that the sample preparation technique is convenient that it neither needs in vacuum or high temperature environments conditions nor requires deposition or coating approaches. All the process can be accomplished in ambient. Therefore, the gold nanorods/NaYF:Yb3+/target molecule system is a perfect object to perform the preliminary experiments for verification.

The specific aim for this project includes:

i) Develop a method to synthesize the gold nanorods with specific plasmonic resonance at the wavelength of 532nm and 1020nm.

ii) Verify the Raman enhancement with the synthesized gold nanorods using Rhodamine 6G and Bovine Serum Albumin (BSA) as a target molecule.

iii) Using anti-stokes/stokes Raman Ratio as a nano thermometry to study the cooling effect on the sample with gold nanorods on the ytterbium doped substrate.

Chapter 2 - Experiment

2.1. Synthesis of gold nanorods

All chemicals were used as received without further purification. Cetyltrimethylammonium bromide (CTAB, ≥ 99%, Sigma Alrich), chloroauric acid ($HAuCl_4 \cdot 3H_2O \geq 99.9\%$, Sigma Alrich), silver nitrate ($AgNO_3$, ≥ 99%, Sigma Alrich), and hydroquinone (≥ 99%, Sigma Alrich). Sodium borohydride ($NaBH_4$, ≥ 98%) was acquired from Fluka. Hydrochloric acid (HCl, certified 1.0 N) and sodium hydroxide (NaOH, 93.0%, Fisher Chemical).

To start the synthesis process, two solutions include seed solution and growth solution must be carefully prepared. The first one is the seed solution, it contains 0.50 mL of 0.010 M Gold chloride trihydrate (HAuCl4 · H2O) with 9.5 mL of 0.10 M Cetyltrimethylammonium bromide (CTAB). The 0.46mL solution contains 0.01M of NaOH and 0.01M of NaBH4 was pre-iced with the refrigirator at 4 degrees Celsius for 2 hours, and then it was quickly added to the seed solution. Simultaneously, an obvious color change from yellow to brown can be observed. After 10mins of rigorous stirring, the seed solution was left in the fume hood statically for 1.5 hours. The next step is to prepare the growth solution which is made of 0.5 mL of 0.01 M HAuCl4 and 8 mL of 0.1 M CTAB as the main component. Then the 40 μL of 0.10 M AgNO3 was added to the growth solution with the falcon tube being gently inverted. Futher, the 30 μL of 1M HCl was also added to the solution, the same mixing process is applied. The final process is to add 0.5 mL of 0.1 M hydroquinone with the same inverted process. Instantly, the solutions will become transparent which means it is ready to use. After obtaining the two solutions correctly, 2.0 mL of the seed solution was added into the growth solution, and left undisturbed for over 24 hours on a 40°C hot plate and subsequently purified the next day through centrifugation at 16,000g for 35 minutes [23–28]. The supernatant was discarded, and the pellet was dispersed in DI water [29].

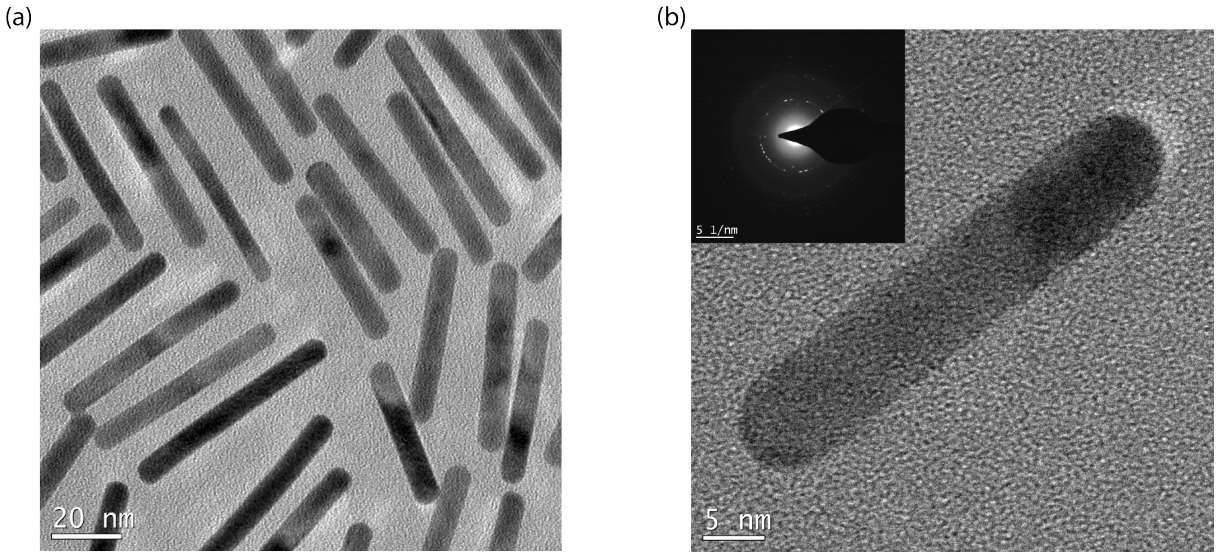

Figure 4. (a) TEM images of the synthesized gold nanorods. (b) Enlarged TEM images of the gold nanorods with diffraction pattern.

As shown in the Figure 3. (a), the synthesized gold nanorods has an average width of 9.6 ± 0.9 nm and the length is about 51.3 ± 5.8 nm, and the aspect ratio is around 6.6 ± 1.6, which corresponds to the theoretical UV-Vis plasmonic resonance at around 1000nm[30]. From Figure 3. (b), the enlarged nanorods with a diffraction pattern can provide the direct evidence that the synthesized material is gold.

2.2. Charaterization

Uv-vis-NIR spectra were measured with a Lambda 950 UV-vis-NIR spctrophotometer (Perkin Elmer Inc., USA). Transmission electron microscopy (TEM) images of AuNR morphology were collected by a Tecnai G2 F20 SuperTwin (Thermo Fisher Scientific Inc., USA). Scanning electron microscopy (SEM) images of AuNR on the NaYF substrate were collected by the Apreo Variable Pressure SEM (Thermo Fisher Scientific Inc., USA). Raman spectrum is collected by HRS-500 Triple Grating Imaging Spectrograph and Scanning Monochromator (Teledyne Princeton Instruments Inc., USA). The Vaccum Raman spectrum is collecting in a Janis ST-500 Continuous Flow Cryostat (Lake Shore Cryotronics Inc., USA) which can be vaccumed by a pump. The TEM image of the gold nanorods in 350℃ sample is heated by Lindberg/Blue M Mini-Mite Tube Furnace (Thermo Fisher Scientific Inc., USA).

2.3. Experimental setup

For various experiments, the preparation methods are different. For the target molecule SERS experiments, the purified gold nanorods solution was drop casted on a silicon wafer and dried in the glove box statically for two hours. Then the target molecule (0.01M of R6G in deionized water, 0.01M of BSA in PBS) was drop casted on top of the gold nanorods, drying process stay the same.

For the laser cooling experiment, firstly the 0.01g NaYF nanoparticles was dispersed in 1.5ml DI water. Before drop casting the solution on the silicon wafer, the mixture needed to be votex for 30 seconds in order to reach thorough dispersion. The sample was dried in the glove box statically for two hours. Next, the gold nanorods solution was drop casted on the silicon wafer covering the NaFY particle region and then the sample was seated in the glove box drying for another two hours. The target 0.01M of R6G is drop casted on top of the gold nanorods in the end. The sample was readied for the Raman test after fully dried.

For the SEM imaging, the condensation of the NaYF solution and the concentration of the gold nanorods solution both needs to be diluted for better analysis. Therefore, the 0.01g NaYF nanoparticles was dispersed in 10ml DI water, and the gold nanorods solution is diluted 3 times before the drop casting process. The preparation process is the same with laser cooling experiment preparation.

For the TEM imaging, the concertration of the gold nanorods solution needs to be diluted further to acquire clearer nanorods morphology. Hence, the gold nanorods solution is diluted 6 times for the TEM sample preparation.

Chapter 3 – Result and discussion

3.1.UV-vis and Scanning Electron Microscopy

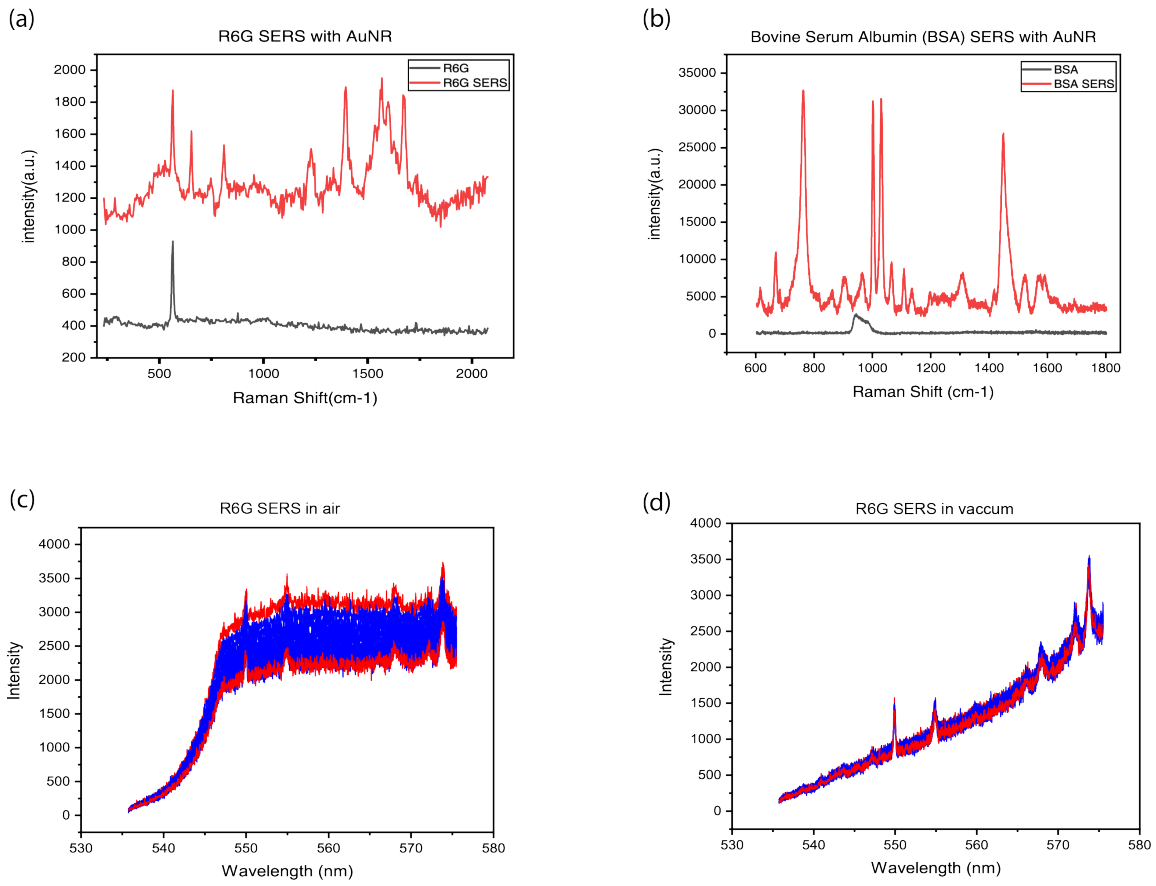

Figure 5. (a) Surface enhanced Raman Spectum (SERS) of target molecule Rhodamine 6G using synthesis AuNR. (b) SERS of target molecule Bovine Serum Albumin using synthesis AuNR. (c) Fifteen frames of Raman spectrum of Rhodamine 6G collected in the ambient showing the peak dropping phenomenon. (d) The same experiment setup collecting the Rhodamine 6G Raman spectrum in vacuum shows that the peaks become stable.

3.2. Surface enhanced Raman Spectrum

As seen in the **Figure 3. (a)**, the spectrum is taken under 30mW of 532nm excitation for 3.2 second. The black line represents the control group with only R6G on the wafer. The Raman data only has one peak at around 564 cm^{-1}, which is not enough for fingerprinting the R6G. The red line stands for the sample with AuNR which has shown the ability of Raman enhancement, the characteristic bands of R6G at 623, 808, 1131, 1225, 1331, 1562, 1611, and 1673 cm^{-1} are clearly evident[5]. One thing is worth keep

in mind is that the non-SERS data has been subtract with the broad photoluminescent peak, at the 532nm excitation, for the R6G specifically, a high intensity photoluminescent (PL) peak occurred which is the major issue for obtaining a Raman spectrum[31]. It is clear that the gold nanorods not only suppress the PL peak, but also enhance the Raman signal at the same time.

While the Raman data collection experiment ongoing, the peak dropping phenomenon was observed. As we can see in the **Figure 3. (c)**, the spectrum was made of 15 frames of the R6G Raman signal, each frame was collected under 1.78mW of 532nm excitation for 3 seconds. The top and buttom red line represent the first and last frame in the data bundle. It is obvious trends that the absolute counts are dropping over 1000 for about 1/3 of the total signal. This peak dropping effect will affect the accuracy of the nano thermometry probe using anti-stoke and stoke Raman ratio as a temperature indicator. The hypothesis that could potentially be used to explain this dropping peaks is that there might be a small amount of singlet oxygen molecule created by the interaction between R6G molecule and incident laser. The singlet oxygen is a very active inorganic chemical, due to their strong oxidation ability. It is normally generated from a photosentitizer molecule which is R6G in this experiment racting with ground state oxygen which is abundant in the ambient atmosphere.

To verify this hypothesis, a control experiment was performed in vacuum in a cryostat. As the **Figure 3. (d)** shown that, under the same circumstances, the top and bottom red line were almost coincided. Therefore, it has proved that the singlet oxygen hypothesis indirectly. If we want to have a more direct evident to show the generation of the dioxygen, a fluorescence reagent experiment needs to perform.

The BSA Raman spectrum is collected under 1% power of 785nm excitation for 30 seconds on a RENISHAW inVia confocal Raman system. As seen in the **Figure 3. (b)**, the black line represents the BSA without any gold nanorods which in other words have no Raman enhancement. And after the gold nanorods has deposite on the surface of the BSA sample, the characteristic Raman peaks at 862, 1002, 1031, 1227, 1625 cm^{-1} is a clear evident[3,7,32]. This experiment also verified the Raman enhancement ability of the synthesized gold nanorods under various laser wavelength. For the BSA sample, it also

contains some background peaks from the reagent in the solution such as the peak at 763 cm^{-1} is assigned for CTAB, and the 905, 967, 1308, 1418 cm^{-1} peaks are from the solution of gold nanorods respectively.

To figure out what peaks have been revealed on the BSA sample. Raman spectrum of different raw reagents from the setup have been proceeded. From **Figure 3. (a), (b), and (c)**, the Raman spectrum of CTAB, critic acid, and PBS shows different peaks which can also be found in the BSA Raman spectrum.

After successfully synthesized the gold nanorods and the progress of Raman enhancement verification. The next step of the project is to explore to what extend the laser will heat up the system which is a critical question to confirm the motivation of this project. In other words, the quantitative experiment must be performed to confirm the laser is heating the system and can cause major damage to the sample. The experiment is designed into three consecutive stages, the first stage is to observe the anti-stoke/stoke ratio due to the anti-stoke Raman signal is very weak in most cases. Since the gold nanorods have been proven to enhance the stokes Raman signal, it is reasonable to conduct the anti-stoke Raman experiment. In other words, if there is not gold nanorods act as a Raman enhancement materials, the anti-stoke Raman spectrum will be too weak to assign as a peak or it is not possible for collecting the data under the optic system in the lab.

After the confirmation of the Raman enhance capability of the gold nanorods, the second stage is to observe the cooling effect. According to the equation, the temperature is related to the anti-stoke and stoke ratio. The higher the ratio the higher the temperature. Although the precise temperature cannot be shown in this equation, the later on calibration experiment can achieve this. Next is the control experiment, to preliminary prove the ratio changing is due to the lanthanide, the experiment used doped NaYF and undoped NaYF as a substrate, both sample are drop casted with the same amount of 50 uL of gold nanosolution, in the mean time the same amount of 20 uL of 0.1 nM of R6G is applied as a target molecule. The Raman test is taken under the same circumstances, the result below should answer the question.

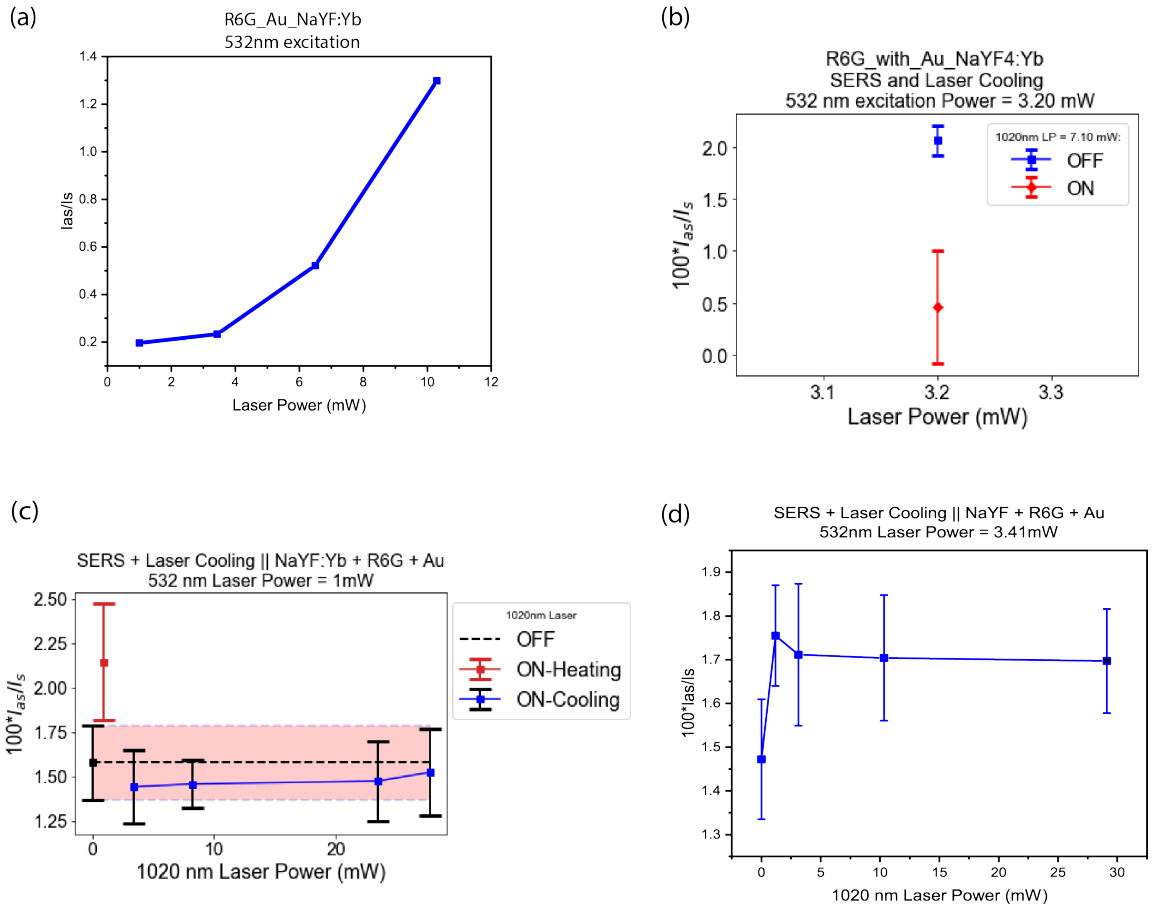

Figure 6. (a) Plot showing the Rhodamine 6G anti-stokes Raman and stokes Raman ratio increasing when the laser power goes up, which indicates that the in-situ temperature is increasing. (b) Plot showing the Rhodamine 6G anti-stokes Raman and stokes Raman ratio significantly dropped when the 7.1mW power dose 1020nm laser excitation was turned on. (c) Acquiring Rhodamine 6G anti-stokes Raman and stokes Raman ratio on acquired on Ytterbium doped NaYF nanoparticle with AuNR substrate with fixed 1mW 532nm laser excitation for Raman spectrum and variate 1020nm laser excitation power from 0 to 28.9mW for laser cooling. (d) Acquiring Rhodamine 6G anti-stokes Raman and stokes Raman ratio on acquired on undoped NaYF nanoparticle with AuNR substrate with fixed 1mW 532nm laser excitation for Raman spectrum and variate 1020nm laser excitation power from 0 to 28.9mW for laser cooling as control experiment.

As shown in **Figure 4. (a)**, the x axis represents the variate 532nm laser power while the y axis shows the anti-stoke/stoke Raman ratio. It is a clear trend that when the laser power rise from 1.3mW to 11.8mW, the ratio rises from 0.2 to 1.3 accordingly. This result reveals that the rising ratio has a high possibility to match the local temperature rising. However, it is worth noting that the ratio and the laser power should be linear in this case. The exponential-like trend can be explained by the good thermal conductivity of the silicon wafer substrate. Namely, when the laser first interacted with the sample, the heat dissipated fast which result in dragging the ratio down from the due value. When the laser continuously heating the sample, the heat dissipation reaches to an equilibrium state which level up the

ratio to the theoretical value. Given the above, the anti-stoke experiment strongly support the idea of using the anti-stokes/stokes Raman ratio as an in-situ nano thermometry, which leads the research to the second stage.

After confirming the accordance between temperature and ratio, the next step is to explore the laser cooling effect on this specific system. As shown in the **Figure 4. (b)**, the blue point was collected with a fixed 3.20mW 532nm green laser, and the red point for comparison is collected with the 7.1mW 1020nm laser co-aligned to the same spot. When the 7.1mW 1020nm laser turned on, the total incident laser power went up while the anti-stokes/stokes Raman ratio become lower which indicated the nano spot on the sample is cooling. This is an inspiring result which shows the 1020nm laser is pumping more energy out of the system that will not only protect the gold nanorods from shape changing, but also prevent the sample from being damaged by the high laser power.

To further investigate and confirm the laser cooling effect, a control experiment using undoped NaYF nanoparticles as a normal group was performed. As seen in the **Figure 4. (c)** and **(d)**, the control experiment both using fixed 532nm incident laser for Raman data collection and using variable 1020nm laser for laser cooling. **Figure 4. (c)** have shown that when the 1020nm laser first turned on, the anti-stokes/stokes Raman ratio went up beyond the original value, which means the temperature become higher. When the 1020nm laser power continue to increase, the ratio went down and lower than the original value. The hypothesis is that within this system, the 1020nm cooling laser has a critical point that it needs to go beyond the power point for compensating the heats introduced into this system, otherwise, the energy will increase rather than decrease. The second laser power is 5.3mW, and as the plot shown, the laser power is higher than the critical point, the system become cooling rather than heating. However, the temperature is not linearly dropping with the 1020nm laser power increasing. Instead, the anti-stokes/stokes Raman ratio come to a steady state. One of the hypotheses is that the laser cooling effect have a bottleneck decided by the efficiency of the lanthanide cooling, but it is not verified yet during this project. It is a complex system involve with multiple incident laser, various nanoparticle and the silicon substrate. The different absorption and heat transfer coefficient from each part of the system makes the situation hard to predict.

For the control experiment, the only difference between the two groups is the yitterbium dopping, which decide the ability for laser cooling. As we could see in Figure 4. (d), the anti-stokes/stokes Raman ratio start to rise the same as the doping sample according to Figure 4. (c), but with increasing laser power, the ratio value drops from 1.75 to 1.7 and stay steadily for the rest of the data point. The hypothesis is that the silicon wafer substrate has a good heat transfer coefficient which can help dissipating the heat from the system in a specific time range. At the beginning of the 1020nm excitation interact with the sample, the heat generated rate is too fast that overriding the heat dissipation, which gives an index to the trend of the plot for up first and drop by a small amount, and then become steady. Although the value of the anti-stokes/stokes Raman ratio is not a linear trend as it present, the overall ratio is higher than the blank point, which means the temperature is going up or at least higher than the doping sample.

3.3. Laser heating

Using anti-stokes/stokes Raman ratio as a nano thermometry to detect the local temperature is a unique technique yet it only provides qualitative analysis which could not act as direct evidence for the status of the gold nanorods after heating. Therefore, a more in-depth TEM analysis would be necessary.

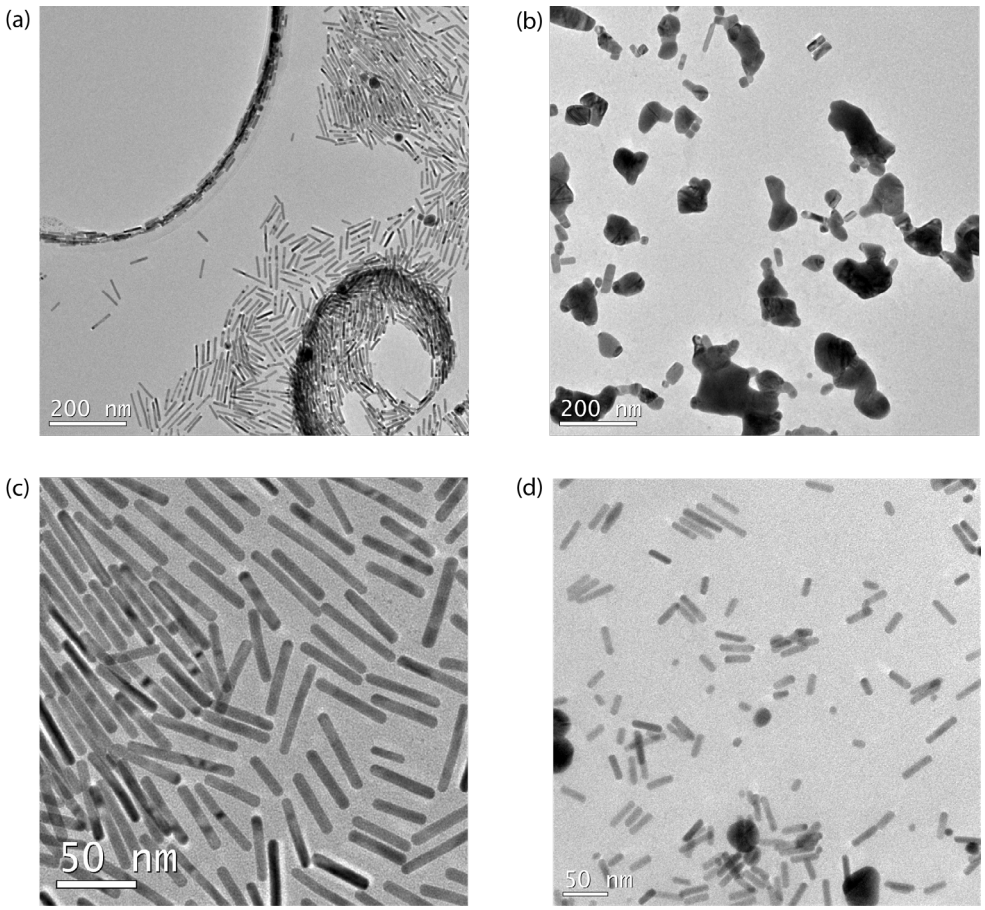

Figure 7. (a) TEM image of gold nanorods on carbon grid. (b) TEM image of the furnace calcined gold nanorods on carbon grid. (c) TEM image of gold nanorods on silicon nitride grid. (d) TEM image of gold nanorods after 500uW of 532nm laser irradiation for 15 seconds on silicon nitride grid.

To begin with, the melting point of gold is a good entry point. Normally, the melting point of bulk gold is 1,064 degrees Celsius, which is beyond the milliwatt scale laser power can reach. However, when the particle size come down to nano scale, the melting point will also become much lower at around 300

degrees Celsius[33–37]. Since the temperature is not that high for the nano gold, it is feasible to use a furnace to heat up the TEM grid for preliminary analysis.

As seen from the Figure 5. (b), the TEM image is taken from a grid with gold seated in a tube furnace that heat up to 300 degrees Celsius by a 10 degrees per minute heating rate and hold for 15 minutes. The shapes of the gold nanorods have a significant change includes many bulky clusters shows up and the rest of the remain gold nanorods become shorter. It is clear that the gold nanorods become melting at or lower than a temperature of 300 degrees Celsius. It follows that the gold nanorods will potentially melting under a low power laser beam. Hence, it is necessary to do some research on the relationship between the gold nanorods shape changing and laser dose. At this time, the silicon nitride TEM grid was chosen due to the normal carbon TEM grid has a high absorption to the 532nm laser and it can be easily burned under various circumstances. As shown in Figure 5. (c), the TEM image shows the gold nanorods before laser irradiation, and in Figure 5. (d), the image represents the gold nanorods being irradiated under only 500uW 532nm excitation for 15 seconds, which is a common laser dose used in a typical Raman data collection experiment.

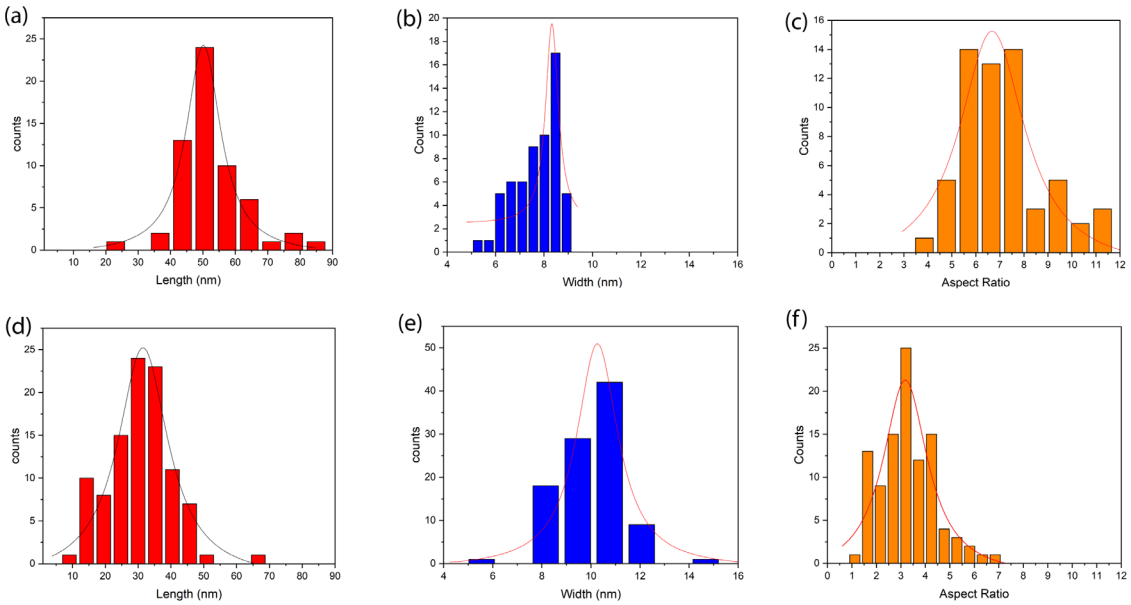

Figure 8. (a) (b) (c) the length, width and aspect ratio distribution respectively of the gold nanorods. (d) (e) (f) the length, width and aspect ratio distribution respectively of the laser heated gold nanorods.

As shown in the Figure 7. (a) and (d), after the laser irradiation, the mean length is shortened from around 50.2nm to 32.4nm while the Figure 7. (b) and (e) tells that the average width of the gold nanorods become slightly larger from 8.8nm to 10.2nm after the laser irradiation, which result in the overall aspect ratio shrinking from 6.8 to 3.2. This result statistically reflects the fact that, even after the low power laser interacted with the gold nanorods, there is enough heat to melt the gold nanorods and have a significant change of the shape.

Chapter 4 – CONCLUSION

4.1. Conclusion

In conclusion, we developed a gold nanorods with specific plasmonic resonance at 532nm and 1020nm, which has the excellent ability to enhance the Raman signal of Rhodamine 6G under 532nm excitation and BSA under 785nm excitation. It potentially enhances the laser cooling performance of NaYF:Yb^{3+} as well. By combing the concept of SERS and laser cooling, it can be a great application for portable Raman spectroscopy devices which could be used in chemical, drugs, viruses and many other Raman compatible reagent detection. Also, the nano thermometry using anti-stokes/stokes Raman ratio to detect the in-situ temperature changing help with the better understanding on how the laser interact with the gold nanorods and the sample. Although, the control experiment leaves a question about why it has the up trend for the 1.3mW laser power point and the all the rest of the ratio are lower than the blank background, it clearly shows that the laser cooling introduced by 1020nm laser is working. Furthermore, the tube furnace was used to investigate the melting temperature for the nano-scale gold. The result is shocking that under 300 degrees Celsius, the gold nanorods has melted and become large chunks of gold cluster. By analyzing the shape changing after the low power laser irradiation, the gold nanorods mean aspect ratio has shifted from 6.6 to 2.1 which strongly support the reason why we need laser cooling technique to protect the gold nanorods and sample from burning.

4.2. Future work

Future work concerns about the details about the interaction between each part of the system. Namely, the interaction between the gold nanorods and the substrate as well as between the laser and sample is important for us to gain improvement to this system, which will help with the process for real applications.

First, in order to reveal why the gold nanorods is melting under a 500uW laser 532nm excitation as well as what is the surface diffusion form of the gold nanorods on the fluride, the quantitative study is needed to show the interaction between the incident laser and gold nanorods on the NaYF:Yb3+ by Discrete Dipole Scattering (DDSCAT) simulation method.

Second, the anti-stokes/stokes Raman ratio is not linked to the exact temperature by the time, which means it is not regards as a nano thermometer technically. Therefore, the temperature calibration experiment needs to perform to show the rigid relationship between the temperature and the anti-stokes/stokes Raman ratio value.

Third, the ultimate goal of this project is to use 1020nm excitation for both Raman spectrum and laser cooling, the next work to do is to perform experiment using only 1020nm laser and collect the Raman spectrum of the target molecule, the cooling data of the NaYF:Yb^{3+} nanoparticle, and the morphology of the gold nanorods after the specific dose of the incident laser.

BIBLIOGRAPHY

1. Pérez-Jiménez, A. I., Lyu, D., Lu, Z., Liu, G. & Ren, B. Surface-enhanced Raman spectroscopy: benefits, trade-offs and future developments. *Chem Sci* **11**, 4563–4577 (2020).
2. Blum, C. *et al.* Understanding tip-enhanced Raman spectra of biological molecules: A combined Raman, SERS and TERS study. *Journal of Raman Spectroscopy* **43**, 1895–1904 (2012).
3. Blum, C. *et al.* Understanding tip-enhanced Raman spectra of biological molecules: A combined Raman, SERS and TERS study. *Journal of Raman Spectroscopy* **43**, 1895–1904 (2012).
4. Martin Fleischmann, B., Hendra, P. J. & James Mcquillan, A. *Raman Spectra from Electrode Surfaces*. (1973).
5. De Barros, A. *et al.* Dynamic Behavior of Surface-Enhanced Raman Spectra for Rhodamine 6G Interacting with Gold Nanorods: Implication for Analyses under Wet versus Dry Conditions. *ACS Appl Nano Mater* **3**, 8138–8147 (2020).
6. Nikoobakht, B., Wang, J. & El-Sayed, M. A. *Surface-enhanced Raman scattering of molecules adsorbed on gold nanorods: off-surface plasmon resonance condition*. www.elsevier.com/locate/cplett.
7. Lin, V. J. C. & Koenig, J. L. *Raman Studies of Bovine Serum Albumin*. *BIOPOLYMERS* vol. 15 (1976).
8. Vigmond, S. J., Ghaemmaghami, V. & Thompson, M. Raman and resonance-Raman spectra of polypyrrole with application to sensor – gas probe interactions. *https://doi.org/10.1139/v95-209* **73**, 1711–1718 (2011).
9. Jayan, H., Pu, H. & Sun, D. W. Recent developments in Raman spectral analysis of microbial single cells: Techniques and applications. *https://doi.org/10.1080/10408398.2021.1945534* **62**, 4294–4308 (2021).
10. Bakker Schut, T. C., Wolthuis, R., Caspers, P. J. & Puppels, G. J. Real-time tissue characterization on the basis of in vivo Raman spectra. *Journal of Raman Spectroscopy* **33**, 580–585 (2002).
11. Kuhar, N., Sil, S., Verma, T. & Umapathy, S. Challenges in application of Raman spectroscopy to biology and materials. *RSC Adv* **8**, 25888–25908 (2018).
12. Norcia, M. A. & Ferlaino, F. Developments in atomic control using ultracold magnetic lanthanides. *Nature Physics 2021 17:12* **17**, 1349–1357 (2021).
13. Norcia, M. A. & Ferlaino, F. New opportunites for interactions and control with ultracold lanthanides. (2021).
14. Zhang, J., Li, D., Chen, R. & Xiong, Q. Laser cooling of a semiconductor by 40 kelvin. *Nature 2013 493:7433* **493**, 504–508 (2013).
15. Maini, A. K. Lasers and optoelectronics: Fundamentals, devices and applications. *Lasers and Optoelectronics: Fundamentals, Devices and Applications* 1–615 (2013)
16. Solid-state Laser Electronics. *Lasers and Optoelectronics* 208–241 (2013)
17. Xia, X. *et al.* Quantum Point Defects for Solid-State Laser Refrigeration. *Advanced Materials* **33**, 1905406 (2021).
18. Jaque, D. & Vetrone, F. Luminescence nanothermometry. *Nanoscale* **4**, 4301–4326 (2012).
19. Nexha, A., Carvajal, J. J., Pujol, M. C., Díaz, F. & Aguiló, M. Lanthanide doped luminescence nanothermometers in the biological windows: strategies and applications. *Nanoscale* **13**, 7913–7987 (2021).
20. Zhou, J., del Rosal, B., Jaque, D., Uchiyama, S. & Jin, D. Advances and challenges for fluorescence nanothermometry. *Nature Methods 2020 17:10* **17**, 967–980 (2020).
21. Jain, P. K., Huang, X., El-Sayed, I. H. & El-Sayed, M. A. Noble metals on the nanoscale: Optical and photothermal properties and some applications in imaging, sensing, biology, and medicine. *Acc Chem Res* **41**, 1578–1586 (2008).

22. Neumann, P. *et al.* Excited-state spectroscopy of single NV defects in diamond using optically detected magnetic resonance. *New J Phys* **11**, 013017 (2009).
23. Xia, Y. *et al. Seed-Mediated Growth Approach for Shape-Controlled Synthesis of Spheroidal and Rod-like Gold Nanoparticles Using a Surfactant Template**. Physical Chemistry of Surfaces* vol. 99 (1999).
24. Gole, A. & Murphy, C. J. Seed-mediated synthesis of gold nanorods: Role of the size and nature of the seed. *Chemistry of Materials* **16**, 3633–3640 (2004).
25. Johnson, C. J., Dujardin, E., Davis, S. A., Murphy, C. J. & Mann, S. Growth and form of gold nanorods prepared by seed-mediated, surfactant-directed synthesis. *J Mater Chem* **12**, 1765–1770 (2002).
26. Sau, T. K. & Murphy, C. J. Room temperature, high-yield synthesis of multiple shapes of gold nanoparticles in aqueous solution. *J Am Chem Soc* **126**, 8648–8649 (2004).
27. Jana, N. R., Gearheart, L. & Murphy, C. J. Wet chemical synthesis of high aspect ratio cylindrical gold nanorods. *Journal of Physical Chemistry B* vol. 105 4065–4067 (2001).
28. Chang, H. H. & Murphy, C. J. Mini Gold Nanorods with Tunable Plasmonic Peaks beyond 1000 nm. *Chemistry of Materials* **30**, 1427–1435 (2018).
29. Scarabelli, L., Sánchez-Iglesias, A., Pérez-Juste, J. & Liz-Marzán, L. M. A 'Tips and Tricks' Practical Guide to the Synthesis of Gold Nanorods. *Journal of Physical Chemistry Letters* **6**, 4270–4279 (2015).
30. Eustis, S. & El-Sayed, M. A. Determination of the aspect ratio statistical distribution of gold nanorods in solution from a theoretical fit of the observed inhomogeneously broadened longitudinal plasmon resonance absorption spectrum. *J Appl Phys* **100**, (2006).
31. Ismail, W. Z. W., Vo, T. P., Goldys, E. M. & Dawes, J. M. Plasmonic enhancement of Rhodamine dye random lasers. *Laser Phys* **25**, (2015).
32. Xiaodan, W. *et al.* Surface-enhanced Raman scattering investigation of bovine serum albumin by Au nanoparticles with different sizes. *J Appl Biomater Funct Mater* **16**, 157–162 (2018).
33. Chankhunthod, N., Aslam, Z., Critchley, K., Evans, S. D. & Brydson, R. Kinetically controlled fabrication of gold nanorods and investigation of their thermal stability via in-situ TEM heating. in *Journal of Physics: Conference Series* vol. 902 (Institute of Physics Publishing, 2017).
34. Taylor, A. B., Siddiquee, A. M. & Chon, J. W. M. Below melting point photothermal reshaping of single gold nanorods driven by surface diffusion. *ACS Nano* **8**, 12071–12079 (2014).
35. Wang, Z. L., Gao, R. P., Nikoobakht, B. & El-Sayed, M. A. Surface reconstruction of the unstable {110} surface in gold nanorods. *Journal of Physical Chemistry B* **104**, 5417–5420 (2000).
36. Ekici, O. *et al.* Thermal analysis of gold nanorods heated with femtosecond laser pulses. *J Phys D Appl Phys* **41**, (2008).
37. Link, S., Wang, Z. L. & El-Sayed, M. A. How does a gold nanorod melt? *Journal of Physical Chemistry B* **104**, 7867–7870 (2000).